ADVANCED MATERIALS
www.advmat.de

Tumor Microenvironment-Triggered Aggregation of Antiphagocytosis ^{99m}Tc-Labeled Fe_3O_4 Nanoprobes for Enhanced Tumor Imaging In Vivo

Zhenyu Gao, Yi Hou, Jianfeng Zeng, Lei Chen, Chunyan Liu, Wensheng Yang, and Mingyuan Gao**

A tumor microenvironment responsive nanoprobe is developed for enhanced tumor imaging through in situ crosslinking of the Fe_3O_4 nanoparticles modified with a responsive peptide sequence in which a tumor-specific Arg-Gly-Asp peptide for tumor targeting and a self-peptide as a "mark of self" are linked through a disulfide bond. Positioning the self-peptide at the outmost layer is aimed at delaying the clearance of the nanoparticles from the bloodstream. After the self-peptide is cleaved by glutathione within tumor microenvironment, the exposed thiol groups react with the remaining maleimide moieties from adjacent particles to crosslink the particles in situ. Both in vitro and in vivo experiments demonstrate that the aggregation substantially improves the magnetic resonance imaging (MRI) contrast enhancement performance of Fe_3O_4 particles. By labeling the responsive particle probe with ^{99m}Tc, single-photon emission computed tomography is enabled not only for verifying the enhanced imaging capacity of the crosslinked Fe_3O_4 particles, but also for achieving sensitive dual modality imaging of tumors in vivo. The novelty of the current probe lies in the combination of tumor microenvironment-triggered aggregation of Fe_3O_4 nanoparticles for boosting the T_2 MRI effect, with antiphagocytosis surface coating, active targeting, and dual-modality imaging, which is never reported before.

Z. Gao, Prof. W. Yang
College of Chemistry
Jilin University
Changchun 130012, China
E-mail: wsyang@jlu.edu.cn
Z. Gao, Prof. Y. Hou, Prof. C. Liu, Prof. M. Y. Gao
Institute of Chemistry
Chinese Academy of Sciences
Bei Yi Jie 2
Zhong Guan Cun
Beijing 100190, China
E-mail: gaomy@iccas.ac.cn
Dr. J. Zeng, L. Chen, Prof. M. Y. Gao
Centre for Molecular Imaging and Nuclear Medicine
School for Radiological and Interdisciplinary Sciences (RAD-X)
Soochow University
Collaborative Innovation Centre of Radiation Medicine
of Jiangsu Higher Education Institutions
Suzhou 215123, China
Prof. M. Y. Gao
School of Chemistry and Chemical Engineering
University of Chinese Academy of Sciences
Beijing 100049, P. R. China

DOI: 10.1002/adma.201701095

Magnetic resonance imaging (MRI) has become a very powerful tool for noninvasively extracting the anatomical structure of the body with high spatial resolution.[1] Nevertheless, due to the low sensitivity of MRI, contrast agents are often required for differentiating the malignant tumor tissue from healthy tissue in the clinic.[2] Magnetic iron oxide nanoparticles have been demonstrated to be an irreplaceable choice as a new types of contrast agents for tumor MR imaging, owing to the outstanding safety profiles apart from the unique tumor-associated enhanced permeation and retention (EPR) effect for nano-objects.[3] Thus, enormous efforts of the past decade have been concentrated on achieving advanced iron oxide contrast agents through precise particle size control,[4] delicate surface modification,[5] and in-depth understanding of the surface modification effects on particle–protein interactions[6] and in particular on the relaxometric properties of the magnetic iron oxide nanoparticles.[7]

To improve the tumor imaging sensitivity, radionuclide-labeled Fe_3O_4 nanoprobes were previously reported, by which the advantages of MR/nuclear imaging modalities can rationally be combined,[8] while incorporating the radionuclide within the crystal lattice of iron oxide nanoparticles were found to be able to further avoid false signals caused by the dissociation of different imaging components.[9] Different from the labeling strategy, simply engineering the size and surface structure of Fe_3O_4 nanoparticles can also give rise to T_1/T_2 dual-modality MRI contrast agents.[7] Along with the multimodality functionalizing strategy, attaching versatile tumor-specific ligand such as antibody,[2b,10] peptide,[11] and folic acid[12] on to the surface of iron oxide particles has also become another main strategy for enhancing the tumor imaging sensitivity of iron oxide nanoparticles and even nanoparticles in general.[13]

Recently, an alternative approach toward sensitive imaging of tumors was proposed through stimuli-induced aggregation of nanoparticles in vivo.[14] Relying on the noncovalent interactions, such as hydrophobic and electrostatic interactions, pH and protease-triggered nanoparticle aggregating systems have been designed, but mostly demonstrated through in vitro

studies.[14a] In contrast, through cycloaddition "click" reaction, matrix metalloproteinases responsive iron oxide nanoparticles were reported for targeted MR imaging through in situ click reactions between the particles modified with azide and alkyne residues, respectively.[14b] In this approach, two complementary nanoparticles are required and the in vivo crosslinking efficiency may suffer from different pharmacokinetic behaviors of nanoparticles bearing different surface structures, apart from the complexity for preparing the two-particle systems. Very recently, Rao and co-workers developed a very interesting caspase3/7-mediated biorthogonal cyclization to assemble Fe_3O_4 nanoparticles for apoptotic tumor MR imaging, which is promising for noninvasively evaluating the chemotherapeutic efficiency of antitumor drugs.[14c,15] Nevertheless, the caspase3/7-activable probes have to first enter the apoptotic tumor cells before they are crosslinked with the aid of glutathione (GSH), the sensitivity for early tumor diagnosis thus suffers.[16]

In general, the stimuli-induced aggregation is favorable for reducing the dose of contrast agent, not only because the retention of particles within tumors will be prolonged, but also because the T_2 effect of iron oxide particles can dramatically be boosted through particle interaction upon aggregation.[17] Although the T_2 effect of iron oxide particles can also be enhanced by increasing the particle size, smaller particles are generally preferred for in vivo applications as they present a longer blood half-life and a shorter biological half-life than larger counterparts.[18] But two major problems remain in the front. One is how to largely evade the clearance of immune system before the nanoparticles reach the tumorous site through blood circulation, and the other is how to effectively induce the nanoparticle aggregation within tumor microenvironment.

To address these issues for precision tumor diagnosis, herein we report a GSH-responsive antiphagocytosis ^{99m}Tc-labeled Fe_3O_4 nanoprobe with active targeting and dual modality imaging capacities. In this probe, an asymmetric poly(ethylene glycol) (PEG) ligand bearing a diphosphate and a maleimide group on different sides (denoted as dp-PEG-mal) was used to PEGylate the magnetite nanocrystals through the diphosphate group, while the remaining maleimide group was used to covalently attach a peptide sequence comprised of Arg-Gly-Asp (RGD) peptide and the self-peptide (Gly-Gly-Asn-Try-Thr-Cys-Glu-Val-Thr-Glu-Leu-Thr-Arg-Glu-Gly-Glu-Thr-Ile-Ile-Glu-Lys) linked through a disulfide bond, as depicted in **Scheme 1**. The self-peptide serves as a stealth coating,[19] for efficiently delivering the magnetite nanoparticles to tumor site after systematic delivery. Upon cleavage of the disulfide bond by GSH highly abundant in tumor microenvironment, RGD takes into play for anchoring the probe onto the surface of cancer cells as its receptor $\alpha_v\beta_3$ is highly expressed by a large number of malignant cancers,[11] while the thiol group remaining on RGD moiety crosslinks the particles through interparticle reaction with the remaining maleimide residues from adjacent particles.

The Fe_3O_4 nanocrystals with an average size of 7.5 ± 0.6 nm, as shown in Figure S1 in the Supporting Information, were prepared through a conventional thermal decomposition method.[20] By replacing the oleate ligand with dp-PEG-mal, biocompatible Fe_3O_4 particles were obtained and shown in Figure S2a (Supporting Information). Via the particle surface

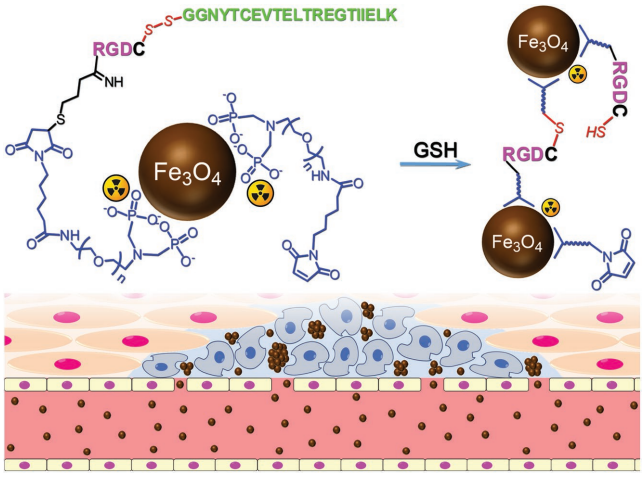

Scheme 1. Schematic drawing of the antiphagocytosis ^{99m}Tc-labeled Fe_3O_4 nanoparticles and their responsiveness to GSH-triggering within tumor microenvironment for forming particle aggregates through interparticle crosslinking reaction.

maleimide residues, the peptide sequence was further covalently attached through click reaction.[21] Through all these processes, the nanoparticles did not present evident changes in both particle size and size distribution. The average number of PEG ligands on each particle was estimated to be approximately 390 and the number of peptide molecules per particle was determined to be approximately 40 based on the results given in Figures S3 and S4 (Supporting Information). For demonstrating the responsive behavior of the probe bearing a disulfide bond in the peptide sequence between RGD and self-peptide moieties (denoted as responsive probe) (Figure S2b, Supporting Information), a control probe was prepared under exactly the same experimental conditions except that the self-peptide was directly linked with RGD with no disulfide linker sitting in between (denoted as nonresponsive probe) (**Figure 1**a).

As shown in Figure 1b, the responsive nanoparticles can effectively be triggered by GSH to form particle aggregates of 69.2 nm on average, after being incubated with 10×10^{-3} M GSH in Tris buffer (pH = 7.4) for 6 h. The dynamic light scattering results confirm that the control probe presents nearly no responsiveness to GSH (Figure 1c), but the responsive probe presents a strong scattering signal at around 220 nm shortly after being incubated with GSH and this signal gradually shifts to 295 nm after 5 h of incubation, as shown in Figure 1d. Meanwhile, the initial scattering peak of the responsive probe at 24 nm remarkably decreases in intensity and slightly splits into two peaks below 100 nm. Very comparable behaviors were also observed by fixing the incubation time while increasing the concentration of GSH. Most importantly, as shown in Figure S5 (Supporting Information), the responsive probe can effectively be triggered to form aggregates even after the GSH concentration was brought down to 0.1×10^{-3} M, substantially lower than the extracellular concentration of GSH in cancers.[16]

The above results suggest that the current responsive probe is very sensitive to GSH and can potentially be used for tumor imaging by taking the advantages of aggregation-enhanced T_2 effect of iron oxide nanoparticles. Although the peptide-coated Fe_3O_4 particles exhibited a moderate transverse relaxivity (r_2) of

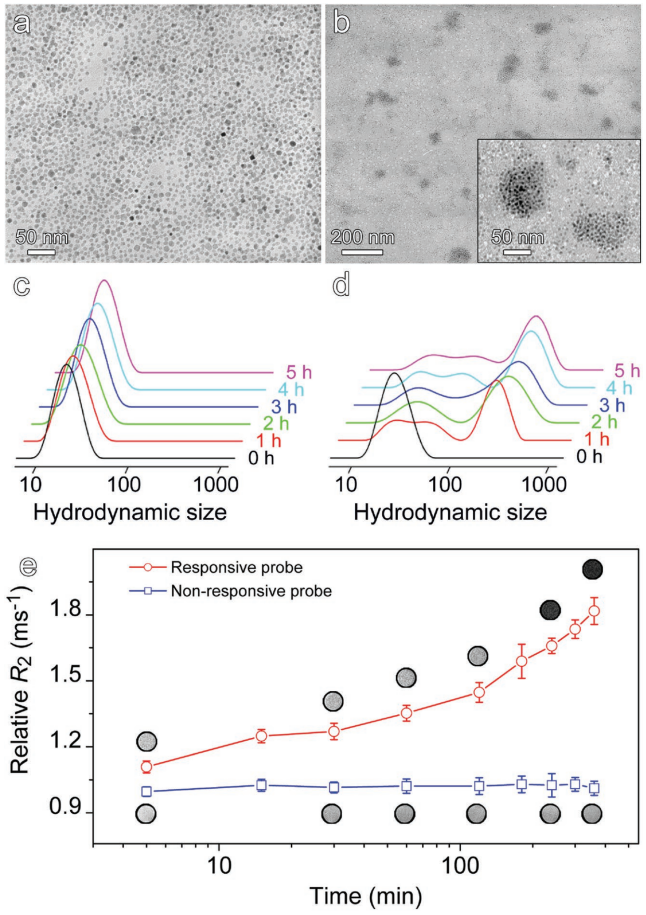

Figure 1. a) TEM (transmission electron microscopy) images of the nonresponsive probe and b) the responsive probe after being treated with GSH. c) Temporal hydrodynamic size profiles of nonresponsive probe and d) responsive probe in react with the GSH treatment, and e) temporal evolutions of the transverse relaxation rate R_2 for responsive probe and nonresponsive control recorded on a 3.0 T MRI scanner during the incubation with GSH (inset: T_2-weighted images of the probe solutions acquired at different incubation time points).

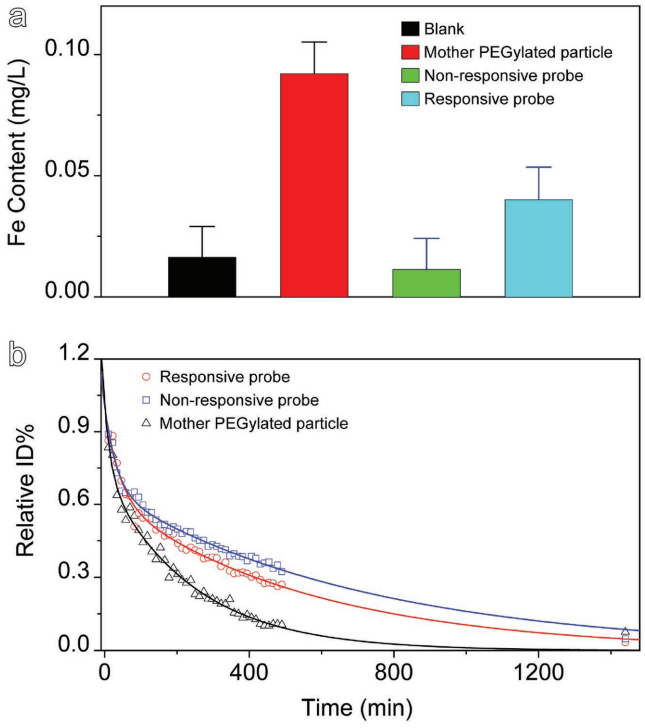

Figure 2. Frame a) Fe contents in RAW264.7 cells treated with the mother particles, nonresponsive probe, and responsive probe, respectively, determined through ICP-AES (Blank represents untreated cells). Frame b) Blood residence profiles of the different probes determined with SPECT overlaid with two-compartment fitting curves for extracting the blood half-lives of different particle probes.

33.4×10^{-3} M^{-1} s^{-1}/1.5 T (Figure S6, Supporting Information), their T_2 effect is significantly enhanced in consequence of the aggregation. As shown in Figure 1e, the transverse relaxation rate R_2 is quickly increased by a factor of more than 1.82 over 6 h incubation, without showing decline. The following phantom imaging results given in the inset of Figure 1e further demonstrate that the current responsive probe presents a significantly stronger aggregation-induced T_2 effect than the probe designed for apoptotic tumor cell imaging through Casp3/7-instructed intracellular aggregation of Fe_3O_4 nanoparticles.[14c] In contrast, the control probe presents nearly unchanged R_2 through the same period of incubation with GSH.

For the nanoprobes capable of tumor active targeting, stealth nature of the nanoprobes enjoys the highest priority for evading the clearance of immune system, so as to maintain high enough probe concentration in bloodstream for continuously infusing the probe particles into tumors. Therefore, in the current probe the self-peptide was adopted as the outmost surface layer for evading the reticuloendothelial (RES) uptake. For showing the antiphagocytosis effect of the self-peptide modification, inductively coupled plasma-atomic emission spectroscopy (ICP-AES) was used for quantitatively evaluating the uptake of various nanoprobes by murine macrophage model cell line, RAW264.7. By determining the Fe content in RAW264.7 cells after being incubated with Fe_3O_4 probes, the effect of self-peptide modification was quantitatively depicted in **Figure 2**a. It is quite obvious that the simple surface PEGylation cannot completely block the macrophage uptake. However, the macrophage uptake can almost completely be suppressed upon the self-peptide modification. Nevertheless, the cell uptake of the responsive probe is slightly compromised, which can reasonably be attributed to the partial detachment of self-peptide moieties with GSH secreted by RAW264.7 cells.[22]

Based on above in vitro studies, the self-peptide modified nanoprobes are expected to exhibit prolonged blood half-life. To verify this hypothesis, the corresponding nanoprobes were labeled with isotope ^{99m}Tc through the diphosphate-anchoring group of the PEG ligand for more accurately display the blood circulation behavior of the nanoprobe as Fe analysis is suffered from high background interference of blood. Moreover, the radioisotope labeling also allows single-photon emission computed tomography (SPECT) imaging for tumor detection. By recording the heart signals acquired at different time points after intravenously delivering the nanoprobes through the tail vein of nude mice, the blood residence behaviors of different nanoprobes were recorded and shown in Figure 2b

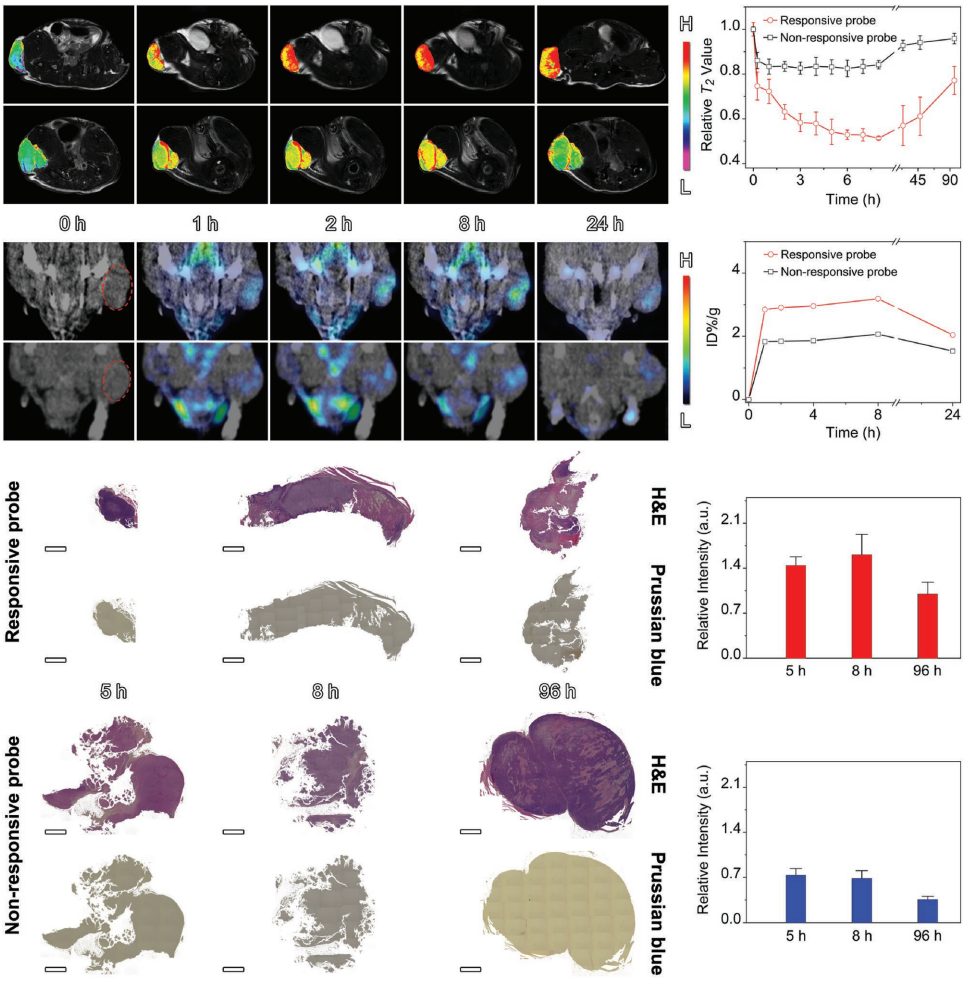

Figure 3. Upper panel: T_2-weighted MR images of tumor-bearing mice acquired before and at different time points after the intravenous injections of the responsive probe (top left) and the nonresponsive probes (bottom left), together with T_2 values extracted from the tumor sites color-coded for better showing the contrast enhancement effects of the particle probes (right); Middle panel: SPECT/CT images of tumor-bearing mice injected with the responsive probe (top left) and the control probe (bottom left), respectively, together with temporal γ-signals of the tumorous areas (right); Lower panel: H&E staining and Prussian blue staining of adjacent slices covering the entire tumorous regions extracted 5, 8, and 96 h postinjection from the tumor-bearing mice received responsive probe (top left) and nonresponsive probe (bottom left), respectively, through intravenous injections (the scale bar corresponds to 1000 µm), together with integrated blue signals of the entire tumorous regions on the right-hand side for showing the temporal difference in tumor uptake of the responsive and nonresponsive probes, respectively, through Prussian blue staining (note: the magnification is too low to see the Prussian blue stains that are better shown under a higher magnification in Figure S8, Supporting Information).

and more detailed fitting results are provided in Table S1 of the Supporting Information. Quite in consistence with the in vitro experimental results, the self-peptide modification largely increases the blood half-life, extracted by fitting the blood residence time with a two-compartment model, from 2.8 h for the mother PEGylated Fe_3O_4 nanoparticles to 8.2 h for the nonresponsive probe and 6.4 h for the responsive probe. This result verifies that the probe design is effective for evading the RES clearance.

On the basis of the improved blood residence performance, the responsive probe was used in detecting tumors in BALB/c nude mice bearing LS180 human colorectal cancer xenografts, with the nonresponsive probe serving as negative control. T_2-weighted MR images acquired before and at different time points after intravenous injection are provided in the top panel of **Figure 3**. Both MRI snapshots and the temporal evolution of the T_2 value of tumorous site support that the GSH-responsive modification can remarkably improve the tumor imaging contrast. Specifically, the T_2 value of the tumorous site starts to decrease shortly after intravenous injection of responsive Fe_3O_4 probe, reaching a signal minimum of approximately 50% at 8 h, while the control probe only gives rise to a decrement of around 18% in T_2 value in consequence of the active targeting effect of the RGD moiety sitting between PEG and self-peptide segments of the ligand and probably EPR effect as well.[7] Moreover, the T_2 value is recovered much slower with ΔT_2 remaining around 20% 96 h postinjection where the T_2 value of the tumor receiving the nonresponsive probe is already recovered. The drastically enhanced T_2 effect clearly demonstrates that the responsive probe possesses an unambiguously ability to improve the tumor imaging contrast owing to GSH-triggered aggregation within tumor microenvironment. Moreover, the

extremely prolonged MRI enhancing effect can reasonably be attributed to in situ crosslinking effect of the responsive probes as larger particles are supposed to be more difficult to be flushed out of tumors than small counterparts.

Since nuclear imaging offers much higher sensitivity than MRI, the ^{99m}Tc-labeled probes were also used for SPECT imaging of tumors from a parallel tumor-bearing mice group for crosschecking the improved imaging sensitivity through particle aggregation. Representative γ-images acquired at 1, 2, 4, 8, and 24 h after the probe was intravenously injected through tail vein were provided in Figure S7 (Supporting Information). The temporal γ-signals of the tumorous areas of both experimental group and control groups are shown in the middle panel of Figure 3. Apparently, the responsive probe presents significantly higher γ-signals than the control probe shortly after they reach the corresponding tumor site. But the enhancement factor at the signal maxima (8 h postinjection) is only of 1.5, substantially lower than the difference in ΔT_2, i.e., 3.1, acquired at the same time point after the responsive probe and control probe were intravenously injected, respectively.

The greatly enhanced T_2 effect of the responsive probe can reasonably be attributed to both aggregation-induced T_2 enhancement and improved retention of the crosslinked particles. To further validate the latter effect, solid tumors were extracted from a parallel group of tumor-bearing mice at different time points postinjection and two adjacent tumor slices were subjected to H&E (hematoxylin-eosin) staining for histopathological analysis and Prussian blue staining for iron assessment, respectively. Based on integrated blue signals from the entire tumorous region after Prussian blue staining, as shown in bottom panel of Figure 3, it can be confirmed that the tumor uptake of the responsive probe is significantly higher than that for the nonresponsive probe. Moreover, the temporal difference in the tumor uptake of Fe_3O_4 nanoparticles is higher than the difference in γ-signals between the experiment and control groups, probably due to the loss of ^{99m}Tc (Figure S7, Supporting Information), but smaller than that in ΔT_2. This is simply because in vivo aggregation help tumors hold more responsive particles, but the γ-signal is simply proportional to the number of particles, while the aggregation of Fe_3O_4 nanoparticles brings in additional effects for MRI, which verifies the benefit of tumor microenvironment-induced aggregation of iron oxide nanoparticles for sensitive imaging of tumors.

In summary, through GSH-triggered aggregation of Fe_3O_4 nanoparticles, the tumor-microenvironment responsive dual-modality imaging probe is constructed with a PEG ligand comprised of RGD peptide and self-peptide sequence coupled with the reducible disulfide linker. Systematic results demonstrate that the self-peptide helps the responsive probes effectively evade the RES uptake after systematic delivery. Upon cleavage of the self-peptide moiety triggered by GSH within tumor, in situ crosslinking of the responsive probes can increase the tumor contrast by a factor of more than 3 in vivo, in comparison with that achieved with noncrosslinkable Fe_3O_4 nanoprobes. In addition, the SPECT imaging capacity is also largely enhanced owing to improved retentions of the crosslinked probe particles. Therefore, it is reasonable to anticipate that the responsive concept demonstrated herein may pave a novel approach for developing advanced probes not only valuable for sensitive tumor imaging but also potentially useful for cancer drug screening by visualizing the tumor-associated abnormal factors.

Experimental Section

Chemicals: The following materials were purchased from Sigma-Aldrich, i.e., $FeCl_3{\cdot}6H_2O$, oleic acid (OA), 1-octadecene (ODE), and 2-iminothiolane hydrochloride. Analytical grade chemical reagents such as ethanol, cyclohexane, and tetrahydrofuran (THF) were purchased from Sinopharm Chemical Reagent Beijing, Co., Ltd. The dp-PEG-mal ligand was a customized product provided by Beijing Oneder Hightech Co. Ltd, the molecular weight of PEG segment is 2000. Murine macrophage cell line RAW264.7, and human colorectal cancer cell line LS180 were obtained from the Oncology School of Peking University. Iron oleate complex was prepared according to a previous report.[20]

Synthesis of Hydrophobic Fe_3O_4 Nanoparticles: Fe_3O_4 nanoparticles of 7.5 nm were synthesized according to a previous report.[20] In brief, 3.6 g (4 mmol) of freshly prepared iron oleate and 3.39 g (4 mmol) of oleic acid were dissolved in 25 mL of 1-octadecene. The resultant solution was heated to 310 °C with a rate of 3.3 °C min^{-1}, and then maintained at 310 °C for 30 min under nitrogen protection. The preparation was terminated by cooling the reaction mixture down to room temperature. The resultant nanoparticles were precipitated by acetone, collected by magnetic separation, washed with acetone several times, and finally redispersed in THF or cyclohexane for further experiments.

Ligand Exchange: As a typical example, 150 mg of dp-PEG-mal was dissolved in 10 mL of THF containing 10 mg hydrophobic Fe_3O_4 nanoparticles. Then, the reaction mixture was heated to 60 °C and kept at this temperature for 12 h under stirring. After that, the Fe_3O_4 nanoparticles were precipitated by cyclohexane, washed with cyclohexane for three times, and then dried under vacuum at room temperature. To remove excess PEG ligand, the PEGylated Fe_3O_4 nanoparticles dissolved in Milli-Q water were further purified through ultrafiltration with 100 kDa MWCO centrifugal filter (Millipore YM-100) for 4 cycles at 6000 g.

Peptide Modification for the PEGylated Fe_3O_4 Nanocrystals: The GSH-responsive nanoprobe was prepared as follows. Typically, 3.13 mg of a RGD/self-peptide conjugate with a sequence of Arg-Gly-Asp-Cys-S-S-MPA-Gly-Gly-Asn-Try-Thr-Cys-Glu-Val-Thr-Glu-Leu-Thr-Arg-Glu-Gly-Glu-Thr-Ile-Ile-Glu-Lys (MPA: mercapto propionic acid) and 0.46 mg of 2-iminothiolane hydrochloride was mixed in 3.0 mL Tris buffer under stirring at room temperature. After reaction for 2 h, 2.5 mL of aqueous solution containing 10 mg of (dp-PEG-mal)-coated Fe_3O_4 nanoparticle was quickly introduced. Through the click reaction between the thiol group on the RGD side formed during above reaction and the maleimide moieties on the surface of the PEGylated Fe_3O_4 nanoparticles, the peptide-modified nanoprobes were formed under stirring for 1 h. The product was then purified by ultrafiltration with 1×PBS (phosphate buffer saline) for 4 cycles using 100 kDa MWCO centrifugal filter (Millipore YM-100) to remove the uncoupled peptide. The control probe bearing no disulfide bond in the peptide sequence was prepared by covalently attaching a peptide with sequence of Arg-Gly-Asp-Cys-Gly-Gly-Asn-Try-Thr-Cys-Glu-Val-Thr-Glu-Leu-Thr-Arg-Glu-Gly-Glu-Thr-Ile-Ile-Glu-Lys onto the particle surface following the above procedures.

^{99m}Tc-Labeling for the Peptide-Modified Fe_3O_4 Nanoprobes: The nanoprobes were labeled with ^{99m}Tc through the chelating effect of the phosphate group of PEG ligand anchoring on the particle surface. Systematic studies have confirmed that ^{99m}Tc ion bridges the phosphate groups from adjacent ligands and helps improve their binding affinity for the underlying particles as well. More detailed results will be published elsewhere. Briefly, 10 µL of $SnCl_2$ (1.0 mg mL^{-1}) solution in 0.1 M HCl was introduced into $Na^{99m}TcO_4$ solution with a radioactivity of 185 MBq (2 mCi). 5 min later, 200 µL of the peptide-modified Fe_3O_4 nanoparticles (1 mg mL^{-1}) solution was introduced into the above mixture. After being kept under stirring at room temperature for 30 min, the resulting solution was subjected to ultrafiltration for 2 cycles with 100 kDa MWCO

centrifugal filter. In this way, the radionuclide-labeled Fe_3O_4 nanoparticles were purified. By determining the radioactivity in filtrate and the residue, the radiolabeling yield was estimated to be around 50%, which results in a specific activity of 5 mCi mg^{-1} for the final particle probe.

In Vitro Antiphagocytosis Assessment of the Peptide-Modified Nanoprobes: ICP-AES was used to evaluate the uptake of nanoprobes by RAW264.7 cells. In brief, RAW264.7 cells were seeded into a 24-well cell culture plate by 8×10^4 cells per well under 100% humidity, and then cultured at 37 °C in an atmosphere containing 5% CO_2 for 24 h. The responsive probe, the nonresponsive probe bearing no disulfide linker, and the mother PEGylated nanoparticle were added into different wells, respectively, and then coincubated with the cells for 24 h at 37 °C under 5% CO_2. After the supernatant was decanted, and the cells were rinsed three times with PBS buffer. Subsequently, the cells were harvested and the Fe content was determined by using ICP-AES after the cells were eroded with 3 M HNO_3.

Animal Tumor Model: The tumor model used was established upon subcutaneous injection of LS180 cells ($\approx 5 \times 10^6$) into male BALB/c nude mice (4–6 weeks old) at the flank region of the hind leg. The tumor imaging studies were carried out when the tumor size reached 5 mm.

In Vivo MR Imaging of Tumor: Nude mice bearing LS180 tumor xenografts were anesthetized and then injected with 100 µL 1 × PBS solution containing nanoprobe or control probes by a dose level of 10 mg Fe^{3+} per kg body weight via tail vein. MR imaging was conducted on a 7.0 T Bruker Biospec animal MRI instrument at designed time points postinjection. The detail imaging parameters were set as follows: FOV (field of view) = 4×4 cm^2, matrix size = 128×128, slice thickness = 1 mm, TE = 15, 30, 45, 60, 75, 90,105, 120 ms, TR = 2500 ms, and NEX = 4. The mice were anesthetized with 1.5% isoflurane delivered via nose cone during the imaging sessions.

SPECT/CT Imaging: The SPECT/CT imaging was carried out with mice carrying comparable tumors in size on an animal SPECT/CT scanner (MILabs, the Netherlands) (scan time: 10 min; frame: 45; FOV: $26 \times 26 \times 70$ mm^3; resolution: 0.4 mm). The injection dose was of 50 mCi per kg weight, corresponding to 10 mg Fe^{3+} per kg body weight. The injected volume was also 100 µL per shot. The acquired SPECT/CT images were reconstructed by a software package provided by MILabs and then fused with a PMOD software. Quantification was performed by selecting the desired organs or tissue as volume of interest using the quantification tool of the PMOD software. The radioactivity of heart was used to monitor the signal of blood, and the tumor region was imaged for evaluating the targeting ability of various probes after quantification.

Histology Analysis: The slices covering the entire tumor region were prepared and two adjacent ones were stained with H&E staining and Prussian blue staining, respectively, following the standard protocols for showing the enhanced retention of the responsive probe after being triggered with GSH in tumor.

All animal experiments reported herein were performed according to a protocol approved by the Peking University Institutional Animal Care and Use Committee.

Supporting Information

Supporting Information is available from the Wiley Online Library or from the author.

Acknowledgements

Z.G. and Y.H. contributed equally to this work. This work was financially supported by the National Natural Science Foundation of China (grant nos. 81471726, 81530057, 81671754, 81571746, and 21403250). All animal experiments reported herein are performed according to a protocol approved by the Peking University Institutional Animal care and use committee.

Conflict of Interest

The authors declare no conflict of interest.

Keywords

antiphagocytosis, Fe_3O_4 nanoparticles, sensitive MRI/SPECT imaging, tumor microenvironment-triggered aggregation

Received: February 24, 2017
Published online: April 12, 2017

[1] M. Bottrill, L. K. Nicholas, N. J. Long, *Chem. Soc. Rev.* **2006**, *35*, 557.
[2] a) P. Caravan, J. J. Ellison, T. J. McMurry, R. B. Lauffer, *Chem. Rev.* **1999**, *99*, 2293; b) J. H. Lee, Y. M. Huh, Y. W. Jun, J. W. Seo, J. T. Jang, H. T. Song, S. Kim, E. J. Cho, H. G. Yoon, J. S. Suh, J. Cheon, *Nat. Med.* **2007**, *13*, 95.
[3] a) R. Qiao, C. Yang, M. Gao, *J. Mater. Chem.* **2009**, *19*, 6274; b) Z. Gao, T. Ma, E. Zhao, D. Docter, W. Yang, R. H. Stauber, M. Gao, *Small* **2016**, *12*, 556.
[4] a) T. Hyeon, S. S. Lee, J. Park, Y. Chung, H. Bin Na, *J. Am. Chem. Soc.* **2001**, *123*, 12798; b) S. H. Sun, H. Zeng, D. B. Robinson, S. Raoux, P. M. Rice, S. X. Wang, G. X. Li, *J. Am. Chem. Soc.* **2004**, *126*, 273; c) N. R. Jana, Y. F. Chen, X. G. Peng, *Chem. Mater.* **2004**, *16*, 3931; d) M. F. Casula, Y. W. Jun, D. J. Zaziski, E. M. Chan, A. Corrias, A. P. Alivisatos, *J. Am. Chem. Soc.* **2006**, *128*, 1675; e) W. W. Yu, J. C. Falkner, C. T. Yavuz, V. L. Colvin, *Chem. Commun.* **2004**, 2306; f) R. Si, Y. W. Zhang, H. P. Zhou, L. D. Sun, C. H. Yan, *Chem. Mater.* **2007**, *19*, 18; g) K. Woo, J. Hong, S. Choi, H. W. Lee, J. P. Ahn, C. S. Kim, S. W. Lee, *Chem. Mater.* **2004**, *16*, 2814; h) Q. Jia, J. Zeng, R. Qjao, L. Jing, L. Peng, F. Gu, M. Gao, *J. Am. Chem. Soc.* **2011**, *133*, 19512.
[5] a) Y. M. Huh, Y. W. Jun, H. T. Song, S. Kim, J. S. Choi, J. H. Lee, S. Yoon, K. S. Kim, J. S. Shin, J. S. Suh, J. Cheon, *J. Am. Chem. Soc.* **2005**, *127*, 12387; b) J. Xie, C. Xu, N. Kohler, Y. Hou, S. Sun, *Adv. Mater.* **2007**, *19*, 3163; c) H. Bin Na, I. S. Lee, H. Seo, Y. I. Park, J. H. Lee, S. W. Kim, T. Hyeon, *Chem. Commun.* **2007**, 5167; d) D. B. Robinson, H. H. J. Persson, H. Zeng, G. X. Li, N. Pourmand, S. H. Sun, S. X. Wang, *Langmuir* **2005**, *21*, 3096; e) N. Nitin, L. E. W. LaConte, O. Zurkiya, X. Hu, G. Bao, *J. Biol. Inorg. Chem.* **2004**, *9*, 706; f) T. Pellegrino, L. Manna, S. Kudera, T. Liedl, D. Koktysh, A. L. Rogach, S. Keller, J. Radler, G. Natile, W. J. Parak, *Nano Lett.* **2004**, *4*, 703; g) W. W. Yu, E. Chang, C. M. Sayes, R. Drezek, V. L. Colvin, *Nanotechnology* **2006**, *17*, 4483; h) W. Cao, X. Lu, Z. Cheng, *Curr. Pharm. Des.* **2015**, *21*, 1908.
[6] S. Liu, Y. Han, R. Qiao, J. Zeng, Q. Jia, Y. Wang, M. Gao, *J. Phys. Chem. C* **2010**, *114*, 21270.
[7] J. Zeng, L. Jing, Y. Hou, M. Jiao, R. Qiao, Q. Jia, C. Liu, F. Fang, H. Lei, M. Gao, *Adv. Mater.* **2014**, *26*, 2694.
[8] S. Liu, B. Jia, R. Qiao, Z. Yang, Z. Yu, Z. Liu, K. Liu, J. Shi, O. Han, F. Wang, M. Gao, *Mol. Pharmaceutics* **2009**, *6*, 1074.
[9] J. Zeng, B. Jia, R. Qiao, C. Wang, L. Jing, F. Wang, M. Gao, *Chem. Commun.* **2014**, *50*, 2170.
[10] F. Hu, L. Wei, Z. Zhou, Y. Ran, Z. Li, M. Gao, *Adv. Mater.* **2006**, *18*, 2553.
[11] J. Xie, K. Chen, H.-Y. Lee, C. Xu, A. R. Hsu, S. Peng, X. Chen, S. Sun, *J. Am. Chem. Soc.* **2008**, *130*, 7542.
[12] C. Sun, R. Sze, M. Zhang, *J. Biomed. Mater. Res., Part A* **2006**, *78A*, 550.

[13] a) L. H. Jing, Y. L. Lin, K. Ding, R. R. Qiao, A. L. Rogach, M. Y. Gao, *Nanotechnology* **2011**, *22*, 505104; b) D. Arosio, L. Manzoni, E. M. V. Araldi, C. Scolastico, *Bioconjugate Chem.* **2011**, *22*, 664; c) H. Y. Liu, X. H. Gao, *Bioconjugate Chem.* **2011**, *22*, 510; d) C. Liu, Y. Hou, M. Gao, *Adv. Mater.* **2014**, *26*, 6922; e) Q. Chen, X. Wang, C. Wang, L. Z. Feng, Y. G. Li, Z. Liu, *ACS Nano* **2015**, *9*, 5223; f) C. Liu, Y. Qi, R. Qiao, Y. Hou, K. Chan, Z. Li, J. Huang, L. Jing, J. Du, M. Gao, *Nanoscale* **2016**, *8*, 12579.

[14] a) D. Chen, N. Li, H. Gu, X. Xia, Q. Xu, J. Ge, J. Lu, Y. Li, *Chem. Commun.* **2010**, *46*, 6708; b) J. Gallo, N. Kamaly, I. Lavdas, E. Stevens, N. Quang-De, M. Wylezinska-Arridge, E. O. Aboagye, N. J. Long, *Angew. Chem., Int. Ed.* **2014**, *53*, 9550; c) Y. Yuan, Z. Ding, J. Qian, J. Zhang, J. Xu, X. Dong, T. Han, S. Ge, Y. Luo, Y. Wang, K. Zhong, G. Liang, *Nano Lett.* **2016**, *16*, 2686; d) C. J. Sun, H. Yang, Y. Yuan, X. Tian, L. M. Wang, Y. Guo, L. Xu, J. L. Lei, N. Gao, G. J. Anderson, X. J. Liang, C. Y. Chen, Y. L. Zhao, G. J. Nie, *J. Am. Chem. Soc.* **2011**, *133*, 8617; e) X. Z. Ai, C. J. H. Ho, J. X. Aw, A. B. E. Attia, J. Mu, Y. Wang, X. Y. Wang, Y. Wang, X. G. Liu, H. B. Chen, M. Y. Gao, X. Y. Chen, E. K. L. Yeow, G. Liu, M. Olivo, B. G. Xing, *Nat. Commun.* **2016**, *7*, 10432; f) X. Cheng, R. Sun, L. Yin, Z. F. Chai, H. B. Shi, M. Y. Gao, *Adv. Mater.* **2017**, *29*, 1604894; g) C. Xie, X. Zhen, Q. L. Lei, R. Ni, K. Y. Pu, *Adv. Funct. Mater.* **2017**, *27*, 1605397.

[15] G. Liang, J. Ronald, Y. Chen, D. Ye, P. Pandit, M. L. Ma, B. Rutt, J. Rao, *Angew. Chem., Int. Ed.* **2011**, *50*, 6283.

[16] R. Franco, J. A. Cidlowski, *J. Biol. Chem.* **2006**, *281*, 29542.

[17] S. Laurent, D. Forge, M. Port, A. Roch, C. Robic, L. V. Elst, R. N. Muller, *Chem. Rev.* **2008**, *108*, 2064.

[18] C. Liu, Z. Gao, J. Zeng, Y. Hou, F. Fang, Y. Li, R. Qiao, L. Shen, H. Lei, W. Yang, M. Gao, *ACS Nano* **2013**, *7*, 7227.

[19] P. L. Rodriguez, T. Harada, D. A. Christian, D. A. Pantano, R. K. Tsai, D. E. Discher, *Science* **2013**, *339*, 971.

[20] J. Park, K. J. An, Y. S. Hwang, J. G. Park, H. J. Noh, J. Y. Kim, J. H. Park, N. M. Hwang, T. Hyeon, *Nat. Mater.* **2004**, *3*, 891.

[21] Y. Hou, J. Zhou, Z. Y. Gao, X. Y. Sun, C. Y. Liu, D. H. Shangguan, W. S. Yang, M. Y. Gao, *ACS Nano* **2015**, *9*, 3199.

[22] P. S. Silverstein, K. L. Audus, N. Qureshi, A. Kumar, *J. Neuroimmune Pharmacol.* **2010**, *5*, 516.